Planet Hunters. VIII. Characterization of 42 Long-Period Exoplanet Candidates from the *Kepler* Archival Data

Ji Wang[1], Debra A. Fischer[1], Alyssa Picard[1], Bo Ma[2], Joseph R. Schmitt[1], Tabetha S. Boyajian[1], Kian J. Jek[3], Daryll LaCourse[3], Christoph Baranec[4], Reed Riddle[5], Nicholas M. Law[6], Chris Lintott[7], Kevin Schawinski [8]

ABSTRACT

The census of exoplanets is quite incomplete for orbital distances larger than 1 AU. Here, we present 42 long-period planet candidates identified by Planet Hunters based on the *Kepler* archival data (Q0-Q17). Among them, 17 exhibit only one transit, 15 have two visible transits and 10 have three visible transits. For planet candidates with only one visible transit, we estimate their orbital periods based on transit duration and host star properties. The majority of the planet candidates in this work (75%) have orbital periods that correspond to distances of 1-3 AU from their host stars. We conduct follow-up imaging and spectroscopic observations to validate and characterize planet host stars. In total, we obtain adaptive optics images for 27 stars to search for possible blending sources. Five stars have stellar companions within 4″. We obtain high-resolution stellar spectra for 7 stars to determine their stellar properties. Stellar properties for other stars are obtained from the NASA Exoplanet Archive and the Kepler Stellar Catalog by Huber et al. (2014). This work provides assessment regarding the existence of planets at wide separations. More than half of the long-period planets in this paper exhibit transit timing variations, which suggest additional components that dynamically interact with the transiting planet candidates. The nature of these components can be determined by follow-up radial velocity and transit observations.

---

[0]This publication has been made possible by the participation of more than 200,000 volunteers in the Planet Hunters project. Their contributions are individually acknowledged at http://www.planethunters.org/authors

[1]Department of Astronomy, Yale University, New Haven, CT 06511 USA

[2]Department of Astronomy, University of Florida, 211 Bryant Space Science Center, Gainesville, FL 32611-2055, USA

[3]Planet Hunter

[4]Institute for Astronomy, University of Hawai'i at Mānoa, Hilo, HI 96720-2700, USA

[5]Division of Physics, Mathematics, and Astronomy, California Institute of Technology, Pasadena, CA 91125, USA

[6]Department of Physics and Astronomy, University of North Carolina at Chapel Hill, Chapel Hill, NC 27599-3255, USA

[7]Oxford Astrophysics, Denys Wilkinson Building, Keble Road, Oxford OX1 3RH

[8]Institute for Astronomy, Department of Physics, ETH Zurich, Wolfgang-Pauli-Strasse 27, CH-8093 Zurich, Switzerland

Subject headings: Planets and satellites: detection - surveys

1. Introduction

Since its launch in March of 2009, the NASA *Kepler* mission has been monitoring ∼160,000 stars in order to detect transiting extrasolar planets with high relative photometric precision (∼20 ppm in 6.5 h, Jenkins et al. 2010). In May 2013, the *Kepler* main mission ended with the failure of a second reaction wheel; however, the first four years of *Kepler* data have led to a wealth of planetary discoveries with a total of 4,175 announced planet candidates[1] (Borucki et al. 2010, 2011; Batalha et al. 2013; Burke et al. 2014). The confirmed and candidate exoplanets typically have orbital periods shorter than 1000 days because at least three detected transits are needed for identification by the automated Transit Planet Search algorithm. Therefore, transiting exoplanets with periods longer than ∼1000 days are easily missed. The detection of short-period planets is further favored because the transit probability decreases linearly with increasing orbital distance. For these reasons, estimates of the statistical occurrence rate of exoplanets tend to focus on orbital periods shorter than a few hundred days (e.g., Fressin et al. 2013; Petigura et al. 2013; Dong & Zhu 2013). Radial velocity (RV) techniques also favor the detection of shorter period orbits, especially for low mass planets. While gas giant planets have been discovered with orbital periods longer than a decade, their smaller reflex velocity restricts detection of sub-Neptune mass planets to orbital radii less than ∼1 AU (Lovis et al. 2011). In principle, astrometric observations favor longer period orbits; however, high precision needs to be maintained over the correspondingly longer time baselines. For shorter periods, the planets need to be massive enough to introduce a detectable astrometric wobble in the star and Gaia should begin to contribute here (Perryman et al. 2001). Microlensing offers sensitivity to planets in wider orbits and has contributed to our statistical knowledge about occurrence rates of longer period planets (e.g., Gaudi 2010; Cassan et al. 2012) and direct imaging of planets in wide orbits is also beginning to contribute important information (Oppenheimer & Hinkley 2009).

Here, we announce 42 long-period transiting exoplanet candidates from the *Kepler* mission. These planet candidates only have 1-3 visible transits and typically have orbital periods between 100 and 2000 days, corresponding to orbital separations from their host stars of 1-3 AU. The candidate systems were identified by citizen scientists taking part in the Planet Hunters project[2] and we have obtained follow-up adaptive optics (AO) images for 27 of these stars and spectroscopic observations for 7 of the host stars in an effort to validate the planet candidates and characterize their host stars. We derive their orbital and stellar parameters by fitting transiting light curves and performing spectral classification.

---

[1] http://exoplanetarchive.ipac.caltech.edu/ as of Mar 23 2015

[2] http://www.planethunters.org/

The Planet Hunters project began in December 2010 as part of the Zooniverse[3] network of Citizen Science Projects. The project displays light curves from the *Kepler* mission to crowd-source the task of identifying transits (Fischer et al. 2012). This method is effective in finding potential exoplanets not flagged by the *Kepler* data reduction pipeline, since human classifiers can often spot patterns in data that would otherwise confuse computer algorithms. The detection efficiency of the volunteers is independent of the number of transits present in the light curve, i.e., they are as likely to identify a single transit as multiple transits in the same lightcurve, however the probability of identifying planets is higher if the transit is deeper. Schwamb et al. (2012) described the weighting scheme for transit classifications. Wang et al. (2013); Schmitt et al. (2014) described the process of vetting planet candidates in detail as well as the available tools on the Planet Hunters website.

The paper is organized as follows. In §2, we model transiting light curves of planet candidates and derive stellar and orbital properties of these candidate systems. In §3, we present adaptive optics (AO) imaging for 27 systems and spectroscopic observations for 7 systems. In §4, we discuss notable candidate systems. Finally, we conclude in §5 with a summary and discussions of future prospects.

2. Planet candidates and their host stars

Planet Hunters identified 42 long-period planet candidates around 38 stars. In this section, we describe the procedures with which we modeled these transit curves and estimated the stellar properties of their host stars. Since 17 planet candidates exhibit only one visible transit, their orbital periods can not be well-determined. We provide a method of constraining the orbital period for a single-transit event based on transit duration and host star properties.

2.1. Modeling Light Curves

We downloaded the *Kepler* light curves from the Mikulski Archive for Space Telescopes (MAST[4]) and detrended the quarterly segments using the autoKep software in the Transit Analysis Package (TAP, Gazak et al. 2012). The light curves were then modeled using TAP which adopts an analytic form for the model described by Mandel & Agol (2002). The free parameters in the model include orbital period, eccentricity, argument of periastron, inclination, the ratio of semi-major axis and stellar radius a/R_*, the planet-star radius ratio R_p/R_*, mid transit time, linear and quadratic limb darkening parameters. We are particularly interested in R_p/R_* and a/R_*. The former is used to determine the planet radius. The latter helps to estimate the orbital periods for planet candidates with only one visible transit. The following equation of constraining orbital period is

[3]https://www.zooniverse.org

[4]http://archive.stsci.edu

derived based on Equation 18 and 19 from Winn (2010):

$$\frac{P}{1\ \mathrm{yr}} = \left(\frac{T}{13\ \mathrm{hr}}\right)^3 \cdot \left(\frac{\rho}{\rho_\odot}\right) \cdot (1-\mathrm{b}^2)^{-\frac{3}{2}}, \tag{1}$$

where P is period, T is the transit duration, i.e., the interval between the halfway points of ingress and egress, ρ is stellar density, $\rho_\odot$ is the solar density, and b is the impact parameter. In a transit observation, the transit duration, T, is an observable that can be parametrized the follow way:

$$T = \frac{1}{\pi} \cdot P \cdot \left(\frac{a}{R_*}\right)^{-1} \cdot \sqrt{(1-\mathrm{b}^2)} \cdot \frac{\sqrt{1-e^2}}{1+e\sin\omega}, \tag{2}$$

where, e is orbital eccentricity and ω is the argument of periastron.

Most of planet candidates in this paper have orbital periods between 100 and 2000 days, and some of these are likely to be in eccentric orbits. Eccentricity affects the transit duration. For example, the transiting duration of a planet on an eccentric orbit can be longer than that for a circular orbit if viewed from the time of apoastron. Unfortunately, it is very difficult to know whether long transit durations are caused by long orbital periods or high eccentricity, especially if the stellar radius is uncertain. However, since 80% of known planets with orbital periods longer than 100 days have eccentricity lower than 0.3[5], we adopt a simplified prior assumption of zero eccentricity in our models. This feeds into our estimates for orbital periods of those systems with only one transit, however the effect is not large. The main uncertainty for the planet period estimation comes from uncertainties in the stellar radius. For example, a typical 40% stellar radius error translates to a ∼40% a/R_* error. Conserving the observable T, the 40% stellar radius error leads to 40% period estimation error according to Equation 2. In comparison, floating the eccentricity between 0 and 0.3 typically changes P by 20%. Therefore, the effect of eccentricity is smaller than the effect of stellar radius error on period estimation. Furthermore, setting eccentricity to zero reduces the number of free parameters by two, i.e., eccentricity and argument of periastron; this facilitates the convergence of the Markov Chains in TAP analysis. This is especially useful when there are only 1-3 transits available to constrain the model. The posterior distribution of the MCMC analysis is used to contain the orbital period (§2.3) for systems that only have single transits.

We report results of light curve modeling for systems with only one observed transit (Table 1), two transits (Table 2), and three transits (Table 3).

2.2. Stellar Mass and Radius

Characterizing host stars for planetary systems helps us to better understand the transiting planets. In particular, the planet radius can be calculated only if stellar radius is estimated. Stellar

[5]http://exoplanets.org/

density is required for estimating the orbital periods for those planets that exhibit only one transit (see Equation 1). We estimate stellar mass and radius in a similar way as Wang et al. (2014): we infer these two stellar properties using the Yale-Yonsei Isochrone interpolator (Demarque et al. 2004). The inputs for the interpolator are $T_{\rm eff}$, $\log g$, [Fe/H], α element abundance [α/H] and stellar age. The first three parameters can be obtained by analyzing follow-up stellar spectra or from the NASA Exoplanet Archive[6] and the updated *Kepler* catalog for stellar properties (Huber et al. 2014). We set [α/H] to be the solar value, zero, and allow stellar age to vary between 0.08 and 15 Gyr. We ran a Monte Carlo simulation to consider measurement uncertainties of $T_{\rm eff}$, $\log g$, [Fe/H]. For stars with spectroscopic follow-up observations (§3.2), the uncertainties are based on the MOOG spectroscopic analysis (Sneden 1973). For stars that are *Kepler* Objects of Interest (KOIs), the uncertainties are from the NASA Exoplanet Archive. We report the1σ ranges for stellar masses and radii in Table 4 along with $T_{\rm eff}$, $\log g$, and [Fe/H].

2.3. Orbital Period

Orbital periods are a fundamental parameter for exoplanets and are often used to understand the prospects for habitability. For systems with more than one visible transit, we determined the orbital period by calculating the time interval between transits. The uncertainty of the orbital period is calculated by propagating the measurement error of the mid transit time of each transit. For systems with only one visible transit, we use Equation 1 to estimate the orbital period P, as a function of the transit duration T, stellar density ρ, and the impact parameter b. T and b can be constrained by modeling the transiting light curve. For instance, T can be measured directly from the transit observation, and b can be inferred by fitting the light curve. On the other hand, ρ can be constrained by stellar evolution model as described in §2.2. Therefore, with knowledge of T, ρ, and b from transit observation and stellar evolution model, we can constrain orbital period for planet candidates with only single transit.

We start with a test TAP run to obtain the posterior distribution of the transit duration T (Equation 2) and impact parameter b. The distribution of stellar density can be obtained from the process as described in §2.2. We then start a Monte Carlo simulation to infer the distribution of orbital period. In the simulation, we sample from T, b and ρ distributions, which result in a distribution of orbital period. We report the mode and 1-σ range of orbital period in Table 1.

We investigate the error of our period estimation using systems with known orbital periods. For the 25 planet candidates with 2-3 transits in this paper, we compare the period ($\bar{P}$) estimated from individual transit and the period (P) based on the interval between mid-transit, which is much more precise than $\bar{P}$. If $\bar{P}$ and P are in agreement within 1-σ error bars, then the method used for single-transit systems would seem to give a reasonable estimate and uncertainty for orbital period.

[6] http://exoplanetarchive.ipac.caltech.edu

The left panel of Fig. 5 shows the distribution of the difference between $\bar{P}$ and P normalized by measurement uncertainty δP, which is calculated as half of the 1-σ range from the Monte Carlo simulation. About 69% of the comparisons are within 1-σ range, which indicates that $\bar{P}$ and P agree for the majority of cases and δP are is a reasonable estimation of measurement uncertainty. The right panel of Fig. 5 shows the fractional error ($\delta P/P$) distribution of the orbital periods estimated from individual transit. The median fractional error is 1.4 and the fractional error is smaller than 50% for 34% of all cases, which suggests that period estimated from individual transit has a large uncertainty, i.e., hundreds of days. This is because of the weak dependence of transit duration on orbital period, i.e., $T \sim P^{1/3}$, a large range of P would be consistent with the measured transit duration. As a result, orbital period uncertainty for systems with single transits is much larger than systems with more than one visible transit. However, the estimation of orbital period provides a time window for follow-up observations.

3. Follow-up Observations

Follow-up observations include AO imaging and spectroscopy of host stars with planet candidates. AO imaging can identify additional stellar components in the system or in the foreground/background. These can be potential sources for flux contamination (e.g., Dressing et al. 2014) or false positives (e.g., Torres et al. 2011). Spectroscopic follow-up observations are used to derive stellar properties that are more reliable than those derived with multi-band photometry. Furthermore, since follow-up observations exclude some scenarios for false positives, the likelihood of a planet candidate being a bona-fide planet can be increased and a planet candidate can be statistically validated (e.g., Barclay et al. 2013). In this section, we describe our AO imaging and spectroscopic follow-up observations. In addition, we discuss sources from which we obtain archival data and information about these planet host stars.

3.1. AO Observation

In total, AO images were taken for 27 stars with planet candidates in this paper. We observed 23 targets with the NIRC2 instrument (Wizinowich et al. 2000) at the Keck II telescope. The observations were made on UT July 18th and August 18th in 2014 with excellent/good seeing between $0.3''$ to $0.8''$. NIRC2 is a near infrared imager designed for the Keck AO system. We selected the narrow camera mode, which has a pixel scale of 10 mas pixel^{-1}. The field of view (FOV) is thus $10''\times10''$ for a mosaic 1K $\times$1K detector. We started the observation in the K_s band for each target. The exposure time was set such that the peak flux of the target is at least 10,000 ADU for each frame, which is within the linear range of the detector. We used a 3-point dither pattern with a throw of $2.5''$. We avoided the lower left quadrant in the dither pattern because it has a much higher instrumental noise than other 3 quadrants on the detector. We continued observations of a target in J and H bands if any stellar companions were found.

We observed 1 target with the PHARO instrument(Brandl et al. 1997; Hayward et al. 2001) at the Palomar 200-inch telescope. The observation was made on UT July 13rd 2014 with seeing varying between 1.0″ and 2.5″. PHARO is behind the Palomar-3000 AO system, which provides an on-sky Strehl of up to 86% in K band (Burruss et al. 2014). The pixel scale of PHARO is 25 mas pixel^{-1}. With a mosaic 1K ×1K detector, the FOV is 25″×25″. We normally obtained the first image in the K_s band with a 5-point dither pattern, which had a throw of 2.5″. The exposure time setting criterion is the same as the Keck observation: we ensured that the peak flux is at least 10,000 ADU for each frame. If a stellar companion was detected, we observed the target in J and H bands.

We observed 11 targets between UT 2014 Aug 23rd and 30th with the Robo-AO system installed on the 60-inch telescope at Palomar Observatory (Baranec et al. 2013, 2014). Observations consisted of a sequence of rapid frame-transfer read-outs of an electron multiplying CCD camera with 0.″043 pixels at 8.6 frames per second with a total integration time of 90 s in a long-pass filter cutting on at 600nm. The images were reduced using the pipeline described in Law et al. (2014). In short, after dark subtraction and flat-fielding using daytime calibrations, the individual images were up-sampled, and then shifted and aligned by cross-correlating with a diffraction-limited PSF. The aligned images were then co-added together using the Drizzle algorithm (Fruchter & Hook 2002) to form a single output frame. The final "drizzled" images have a finer pixel scale of 0.″02177/pixel.

The raw data from NIRC2 and PHARO were processed using standard techniques to replace bad pixels, flat-field, subtract thermal background, align and co-add frames. We calculated the 5-σ detection limit as follows. We defined a series of concentric annuli centering on the star. For the concentric annuli, we calculated the median and the standard deviation of flux for pixels within these annuli. We used the value of five times the standard deviation above the median as the 5-σ detection limit. We report the detection limit for each target in Table 5. Detected companions are reported in Table 6.

3.2. Spectroscopic Observation

We obtained stellar spectra for 7 stars using the East Arm Echelle (EAE) spectrograph at the Palomar 200-inch telescope. The EAE spectrograph has a spectral resolution of ∼30,000 and covers the wavelength range between 3800 to 8600 Å. The observations were made between UT Aug 15th and 21st 2014. The exposure time per frame is typically 30 minutes. We usually obtained 2-3 frames per star and bracketed each frame with Th-Ar lamp observations for wavelength calibration. Because these stars are faint with *Kepler* magnitudes mostly ranging from 13 to 15.5 mag, the signal to noise ratio (SNR) of their spectra is typically 20-50 per pixel at 5500 Å.

We used IDL to reduce the spectroscopic data to get wavelength calibrated, 1-d, normalized spectra. These spectra were then analyzed by the newest version of MOOG (Sneden 1973) to derive stellar properties such as effective temperature ($T_{\rm eff}$), surface gravity ($\log g$) and metallicity

[Fe/H] (Santos et al. 2004). The iron line list used here was obtained from Sousa et al. (2008) excluding all the blended lines in our spectra due to a limited spectral resolution. The measurement of the equivalent widths was done systematically by fitting a gaussian profile to the iron lines. The equivalent widths together with a grid of Kurucz Atlas 9 plane-parallel model atmospheres (Kurucz 1993) were used by MOOG to calculate the ion abundances. The errors of the stellar parameters are estimated using the method described by Gonzalez & Vanture (1998). The targets with spectroscopic follow-up observations are indicated in Table 4.

3.3. Archival AO and Spectroscopic Data From CFOP

For those targets for which we did not conduct follow-up observations, we searched the *Kepler* Community Follow-up Observation Program[7] (CFOP) for archival AO and spectroscopic data. We found that only one target had AO images from CFOP. KIC 5857656 was observed at the Large Binocular Telescope on UT Oct 3rd 2014, but the image data was not available. A total of 14 of targets had spectroscopic data based on CFOP, but only 8 of them had uploaded stellar spectra. We used the spectroscopically-derived stellar properties for these stars in the subsequent analyses.

3.4. Stars without AO and Spectroscopic Data

For stars without AO and spectroscopic data, we obtained their stellar properties from the NASA Exoplanet Archive if they were identified as *Kepler* Objects of Interest (KOIs). If the stars are not KOIs, then we obtained their stellar properties from the update *Kepler* catalog for stellar properties (Huber et al. 2014).

4. Planet Candidates and Notable Systems

Fig. 6 shows a scatter plot of planet radii and orbital periods found by *Kepler*. Most of the known KOIs (88%) have orbital periods shorter than 100 days so the planet candidates discovered by the Planet Hunters help extend the discovery space into the long period regime. We emphasize that we have included in this paper planet candidates with one or two observed transits, which may have higher false positive rate and would otherwise excluded by the *Kepler* pipeline. This approach enables the Planet Hunters project to be more sensitive to long-period planet candidates, allowing us to explore a larger parameter space. Below we discuss some notable systems.

[7]https://cfop.ipac.caltech.edu

4.1. Single-Transit Systems

3558849 This star is listed as KOI-4307 and has one planet candidate with period of 160.8 days, but KOI-4307.01 does not match with the single transit event. Therefore this is an additional planet candidate in the same system.

5010054 This target is not in the threshold crossing event (TCE) or KOI tables. Three visible transits are attributed to two planet candidates. The first two at BKJD 356 and 1260 (Schmitt et al. 2014) are from the same object (they are included in the following Double-Transit Systems section). The third transit at BKJD 1500 is different in both transit depth and duration, so it is modeled here as a single transit from a second planet in the system.

5536555 There are two single-transit events for this target (BKJD 370 and 492). We flag the one at BKJD 370 as a cosmic-ray-induced event. It is caused by Sudden Pixel Sensitivity Dropout (SPSD, Christiansen et al. 2013; Kipping et al. 2015). After a cosmic ray impact, a pixel can lose its sensitivity for hours, which mimics a single-transit event. A cosmic ray hitting event is marked as a SAP_QUALITY 128 event when cosmic ray hits pixels within photometric aperture and marked as a SAP_QUALITY 8192 event when cosmic ray hits adjacent pixels of a photometric aperture. The single-transit event at BKJD 370 coincides with with a SAP_QUALITY 128 event, so we caution that it may be an artifact. However, the single-transit event at BKJD 492 is still a viable candidate. Single-transit events that are caused by SPSD are also found for other *Kepler* stars. We list here the SPSDs found by Planet Hunters and the associated BKJDs: KIC 9207021 (BKJD 679), KIC 9388752 (BKJD 508), and KIC 10978025 (BKJD 686).

8540376 There are only two quarters of data for this target (Q16 and Q17). However, there are three planet candidates in this system. One starts at BKJD 1499.0 and has an orbital period of 10.7 days. One has only two observed transits with an orbital period of 31.8 days. The two-transit system will be discussed in the following section (§4.2). There is a single-transit event (BKJD 1516.9), which appears to be independent of the previous two planet candidates. This single-transit event would be observed again soon because its orbital period has a 1-σ upper limit of 114.1 days.

9704149 There is a second possible transit at BKJD 1117, but only ingress is recorded here and the rest of the transit is lost due to a data gap. If the second transit is due to the same object, then the orbital period is 697.3 days, which is at odds with the estimated period at 1199.3 days.

10024862 In addition to the single transit event, there is also a second object with three visible transits (P = 567.0 days, see §4.3). The triple-transit system was also reported in Wang et al. (2013), but there were only two visible transits at that time.

10403228 This is a transit event from a planet around a M dwarf. Despite the deep transit ($\sim$5%), the radius of the transiting object is within planetary range (R_P = 9.7 $R_\oplus$). However, the transit is v-shaped, suggesting a grazing transit and the true nature of the transiting object is uncertain. For the M star, we adopt stellar mass and radius from Huber et al. (2014) which uses

the Dartmouth stellar evolution model (Dotter et al. 2008).

10842718 The orbital period distribution given the constraints from transit duration and stellar density (§2.3) has two peaks. One is at ∼1630 days, the other one is at ∼10,000 days. The bimodal distribution suggests that the orbital period of this transiting object could be much longer than reported in Table 1, however the probability for a transiting planet with a period of ∼10,000 days is vanishingly low, giving stronger weight to the shorter period peak.

4.2. Double-Transit Systems

3756801 This object is first mentioned in Batalha et al. (2013) and designated as KOI-1206. Surprisingly, it appears that only one transit was detected by Batalha et al. (2013). It does not appear in the *Kepler* TCE table because a third transit was not observed.

5732155 A stellar companion has been detected in K_S band that is 4.94 magnitudes fainter. The separation of the stars is $1''$ (Table 6). The flux contamination does not significantly change the transit depth and thus does not affect planet radius estimation. The stellar companion is so faint that even a total eclipsing binary would not yield the observed transit depth.

6191521 This target is listed as KOI-847 and has one planet candidate with orbital period of 80.9 days. Here, we report a second, longer-period planet candidate that was not previously detected in the system.

8540376 There are only two quarters of data for this target (Q16 and Q17), but there are three planet candidates in this system. The longer period single-transit event has been discussed in §4. The double-transit event starts at BKJD 1520.3 and has a period of 31.8 days. The shortest period planet (10.7 days) has transits that begin at BKJD 1499.0.

8636333 This target is listed as KOI-3349 and has two planet candidates. One is KOI-3349.01 with period of 82.2 days; the other one was reported in Wang et al. (2013) with period of 804.7 days. Here, we report the follow-up observations for this star: a fainter stellar companion has been detected in H and K_S bands (Table 6) with differential magnitudes of 1.58 and 1.71 in these filters respectively. We estimate their *Kepler* band magnitudes to be different by $\sim$ 3 mag. Based on Fig. 11 in Horch et al. (2014), a correction for the radius of the planet that accounts for flux from the stellar companion would increase the planet radius by a small amount, ∼3%. However, if the two candidates are transiting the fainter secondary star, then their radii would increase by a factor of ∼3. In this case, although the radii for both candidates would remain in planetary range, the longer-period candidate would be at the planetary radius threshold.

9214713 This target is listed as KOI-422 and has one planet candidate that matches with the double-transit event found by Planet Hunters.

9663113 This target is listed as KOI-179 and has two planet candidates. One is KOI-179.01

with period of 20.7 days. KOI-179.02 was reported in Wang et al. (2013) with period of 572.4 days with two visible transits. The expected third transit at BKJD 1451 is missing, but the expected position is in a data gap.

10255705 This target was reported in Schmitt et al. (2014). Follow-up AO observation shows that there is a nearby stellar companion (Table 6). The companion is ∼2 mag fainter in *Kepler* band. If the planet candidate orbits the primary star, then the planet radius adjustment due to flux contamination is small. If the planet candidate orbits around the newly detected stellar companion, then the planet radius is revised upward by a factor of ∼2 (Horch et al. 2014), but the adjusted radius is still within planetary range.

10460629 This target is listed as KOI-1168 and has one planet candidate that matches with the double-transit event. There are two deep v-shaped dips in the lightcurve at BKJD 608.3 and 1133.3, likely indicating an eclipsing binary within the planet orbit. These v-shaped transits are so deep (about 13%) that they could easily be followed up from the ground. If the planet interpretation is correct for the other two transit events, then this could be an circumbinary planet candidate.

10525077 This target is listed as KOI-5800 and has one planet candidate with period of 11.0 days. The second planet candidate was reported in Wang et al. (2013) with period of 854.1 days. There are two transits at BKJD 355.2 and 1189.3. In between these two transits, there is a data gap at 762.3, preventing us from determine whether the orbital period is 854.1 days or half of the value, i.e, 427.05 days.

12356617 This target is listed as KOI-375 and has one planet candidate that matches with the double-transit event. Follow-up AO observation shows that there is one faint stellar companion at 3.12″ separation. If the transit occurs for the primary star, the radius adjustment due to flux contamination is negligible. If the transit occurs for the secondary star, then this is a false positive.

4.3. Triple-Transit Systems

5437945 This target is listed as KOI-3791and has two planet candidates in 2:1 resonance. KOI-3791.01 was reported in Wang et al. (2013) and Huang et al. (2013). The fourth transit appears at BKJD 1461.8.

5652983 This target is listed as KOI-371 and has one planet candidate that matches with the triple-transit event. The radius of the transiting object is too large to be a planet, and thus the triple-transit event is a false positive, which is supported by the notes from CFOP that large RV variation has been observed.

6436029 This target is listed as KOI-2828 and has two planet candidates. KOI-2828.02 with period of 505.5 days matches the triple-transit event. KOI-2828.02 was reported in Schmitt et al. (2014), but there were only two visible transits.

7619236 This target is listed as KOI-5205 and has one planet candidate that matches with the triple-transit event. It exhibits significant transit timing variations (TTVs). The time interval between the first two transits is different by ∼27 hours from the time interval between the second and the third transit.

8012732 This object was reported in Wang et al. (2013). It exhibits significant TTVs. The time interval between the first two transits is different by ∼20 hours from the time interval between the second and the third transit.

9413313 This object was reported in Wang et al. (2013). It exhibits significant TTVs. The time interval between the first two transits is different by ∼30 hours from the time interval between the second and the third transit.

10024862 This object was reported in Wang et al. (2013), but only two transit were observed then. The third transit is observed at BKJD 1493.8. It exhibits significant TTVs. The time interval between the first two transits is different by ∼41 hours from the time interval between the second and the third transit.

10850327 This target is listed as KOI-5833 and has one planet candidate that matches with the triple-transit event. The object was reported in Wang et al. (2013), but there were only two transit observed then.

11465813 This target is listed as KOI-771 and has one planet candidate that matches with the triple-transit event. The transit depth is varying. This target also has a single transit at BKJD 1123.5. A stellar companion has been detected (Table 6). From the colors of the companion, we estimate the differential magnitude to be 0.7 mag. The radius of the object would be revised upward by 23% or 150% depending on whether the object orbits the primary or the secondary star. In either case, it is likely that this object is a false positive.

11716643 This target is listed as KOI-5929 and was reported in Wang et al. (2013), but there were only two transits observed then. It exhibits TTVs. The time interval between the first two transits is different by ∼2.7 hours from the time interval between the second and the third transit.

4.4. Notable False Positives

In addition to the systems with single-transit events flagged as SPSDs in §4.1, we list other transiting systems that are likely to be false positives.

1717722 This target is listed as KOI-3145 with two known planet candidates. Neither candidate matches the single transit event at BKJD 1439. This single transit is likely spurious, as pixel centroid offset between in- and out-of-transit are seen for this transit.

3644071 This target is listed as KOI-1192 and has one false positive (02) and one candidate (01). The epoch for candidate KOI-1192.01 matches with the epoch of the single transit event

in this paper. According to notes on CFOP, the KOI-1192 event is "due to video crosstalk from an adjacent CCD readout channel of the image of a very bright, highly saturated star". This effect causes the varying transit depth and duration. The explanation is further supported by the apparent pixel offset between in- and out-of-transit for both KOI-1192.01 and KOI-1192.02. So KOI-1192.01 is also likely to be a false positive.

10207400 This target is currently not in either the Kepler KOI or TCE tables. There is a pixel centroid offset between in- and out-of-transit.

5. Summary and Discussion

5.1. Summary

We report 42 long-period planet candidates around 38 *Kepler* stars. These planet candidates are identified by the Planet Hunters based on the archival *Kepler* data from Q0 to Q17. We conduct AO imaging observations to search for stellar companions and exclude false positive scenarios such as eclipsing binary blending. In total, we obtain AO images for 27 stars. We detect stellar companions around five stars, KIC 5732155, KIC 8636333 (KOI 3349), KIC 10255705, KIC 11465813 (KOI 771), and KIC 12356617 (KOI 375). The properties of these stellar companions are given in Table 6. For those stars with non-detections, we provide AO sensitivity limits at different angular separations (Table 5). We obtain high-resolution spectra for a total of 7 stars. We use the stellar spectra to infer stellar properties such as stellar mass and radius which are used for orbital period estimation for single-transit events. The stellar properties of planet host stars are given in Table 4. We model the transiting light curves with TAP to obtain their orbital parameters. Table 1, Table 2 and Table 3 give the results of light curve modeling for single-transit, double-transit, and triple-transit systems, respectively.

5.2. A Dynamically-Unstable Circum-Binary Planetary System: KIC 10460629

KIC 10460629 may be an extreme circumbinary planetary system if confirmed with a $P = 856.7$ days planet and a $P = 525$ days eclipsing binary star. The ratio of semi-major axis of the transiting planet to the eclipsing secondary star is $\sim$1.4. The tight orbital configuration makes the system dynamically unstable. According to Equation 3 in Holman & Wiegert (1999), the minimum semi-major axis ratio for a stable orbit around a binary star is 2.3 for a binary with $e = 0$ and $\mu = 0.5$, where μ is the mass ratio of the primary to the secondary star estimated from the transit depth (13%). Therefore, KIC 10460629 should be dynamical unstable. Furthermore, the minimum semi-major axis ratio increases with increasing eccentricity, which makes the systems even more unstable for eccentric orbits based on the criterion from Holman & Wiegert (1999).

Follow-up observations are necessary to determine the nature of this transiting system. Long

time-baseline RV observations can determine the orbital parameters of the secondary star, though the precision of RV measurements may not be adequate to map out the orbit of the transiting planet candidate with a Neptune-size ($R_p = 3.8 \pm 0.8$ $R_\oplus$) given the low-mass and the faintness of the host star ($K_P = 14.0$). Ground-based transiting follow-up observations can certainly catch the transit of the secondary star at 13% depth. The next transit of the secondary star will on UT June 1st 2016. The transit depth of the planet candidate is ∼800 ppm, which can be detected by ground-based telescopes. The next transit of the planet candidate will be on UT August 30 2016. Because of the long orbital period, it requires years' observations to gather transiting data for this system. However, once adequate data are available, we can start to look for additional planets in the same system via TTVs and measure orbital configuration and dynamical masses via photo-dynamical modeling (Carter et al. 2012).

5.3. Evidence of Additional Planets in Systems with Long-Period Transiting Planets

TTVs indicate the likely presence of additional components in the same system that dynamically interacting with transiting planet candidates. For the 10 systems with 3 visible transits for which we can measure TTVs, 50% (5 out of 10) exhibit TTVs ranging from ∼2 to 40 hours. Excluding two likely false positives, KIC 5652983 (large RV variation) and KIC 11465813 (blending), the fraction of systems exhibiting TTVs goes up to 68%. All such systems host giant planet candidates with radii ranging from 4.2 to 12.6 $R_\oplus$. This result suggests that most long-period transiting planets have at least one additional companion in the same system. This finding is consistent with the result in Fischer et al. (2001) that almost half (5 out of 12) of gas giant planet host stars exhibit coherent RV variations that are consistent with additional companions. This finding is further supported by a more recent study of companions to systems with hot Jupiters (Knutson et al. 2014; Ngo et al. 2015), in which the stellar and planetary companion rate of hot Jupiter systems is estimated to be ∼50%. While we emphasize the different planet populations between previous studies (short-period planets) and systems reported in this paper (long-period planets), the companion rate for stars with gas giant planets is high regardless of the orbital period of a planet.

Dawson & Murray-Clay (2013) found that giant planets orbiting metal-rich stars show signatures of planet-planet interactions, suggesting that multi-planet systems tend to favorably reside in metal-rich star systems. We check the metallicities of the five systems exhibiting TTVs. The median metallicity is 0.07 ± 0.18. In comparison, the median metallicity for the entire sample is -0.06 ± 0.38 dex. While there is a hint that the TTV sample is more metal rich, the large error bars and the small sample prevent us from further studying the metallicity distribution of systems exhibiting TTVs. However, studying the metallicity of planet host stars remains a viable tool and future follow-up observations would allow us to use the tool to test planet formation theory.

5.4. The Occurrence Rate of Long-Period Planets

The presence of long-period planets may affect the evolution of multi-planet systems by dynamical interaction (e.g., Rasio & Ford 1996; Dong et al. 2014). The dynamical effects result in observable effects such as spin-orbit misalignment which provides constraints on planet migration and evolution (e.g., Winn et al. 2010). Therefore, measuring the occurrence rate of long-period planets is essential in determine their role in planet evolution. Cumming et al. (2008) estimated that the occurrent rate is 5-6% per period decade for long-period gas giant planets. Knutson et al. (2013) estimated that $51\% \pm 10\%$ of hot-Jupiter host stars have an additional gas giant planet in the same system. However, these studies are sensitive to planets with mass higher than $\sim$0.3 Jupiter mass. The *Kepler* mission provides a large sample of small planets (likely to be low-mass planets), which can be used to infer the occurrence rate for small, long-period planets. However, such analysis is limited to periods up to $\sim$500 days (Dong & Zhu 2013; Petigura et al. 2013; Rowe et al. 2015). The upper limit is due to the 3-transit detection criterion for *Kepler* planet candidates. With the long-period planet candidates in this paper, we will be able to probe the occurrence rate of planets between 1 and 3 AU. To accomplish this goal, a proper assessment of planet recovery rate of the Planet Hunters is required. The framework has already been provided by Schwamb et al. (2012) and this issue will be addressed in a future paper. Estimating the occurrence rate of Neptune to Jupiter-sized planets between 1 and 3 AU will be an important contribution of Planet Hunters to the exoplanet community.

5.5. K2 and TESS

The current K2 mission and future TESS (Transiting Exoplanet Survey Satellite) missions have much shorter continuous time coverage than the *Kepler* mission. Each field of the K2 mission receives $\sim$75 days continuous observation (Howell et al. 2014). For the TESS mission, the satellite stays in the same field for 27.4 days (Ricker et al. 2015). Despite longer time coverage for a portion of its field, the majority of sky coverage of TESS will receive only 27.4 days observation. Given the scanning strategy of these two missions, there will be many single-transit events. Estimating the orbital periods for these events is crucial if some the targets with single transit have significant scientific value, e.g., planets in the habitable zone. More generally, estimating orbital period helps to predict the next transit and facilitates follow-up observations, especially for those searching for the next transit. Once more than one transits are observed, more follow-up observations can be scheduled such as those aiming to study transiting planets in details, e.g., CHEOPS (CHaracterising ExOPlanet Satellite) and JWST (James Webb Space Telescope).

Acknowledgements We are grateful to telescope operators and supporting astronomers at the Palomar Observatory and the Keck Observatory. Some of the data presented herein were obtained at the W.M. Keck Observatory, which is operated as a scientific partnership among the California Institute of Technology, the University of California and the National Aeronautics and Space Ad-

ministration. The Observatory was made possible by the generous financial support of the W.M. Keck Foundation. The research is made possible by the data from the *Kepler* Community Follow-up Observing Program (CFOP). The authors acknowledge all the CFOP users who uploaded the AO and RV data used in the paper. This research has made use of the NASA Exoplanet Archive, which is operated by the California Institute of Technology, under contract with the National Aeronautics and Space Administration under the Exoplanet Exploration Program.

The Robo-AO system was developed by collaborating partner institutions, the California Institute of Technology and the Inter-University Centre for Astronomy and Astrophysics, and with the support of the National Science Foundation under Grant Nos. AST-0906060, AST-0960343 and AST-1207891, the Mt. Cuba Astronomical Foundation and by a gift from Samuel Oschin.C.B. acknowledges support from the Alfred P. Sloan Foundation. KS gratefully acknowledges support from Swiss National Science Foundation Grant PP00P2_138979/1

Facilities: PO:1.5m (Robo-AO)

REFERENCES

Baranec, C., et al. 2013, Journal of Visualized Experiments, 72, e50021

—. 2014, ApJ, 790, L8

Barclay, T., et al. 2013, ApJ, 768, 101

Batalha, N. M., et al. 2013, ApJS, 204, 24

Borucki, W. J., et al. 2010, Science, 327, 977

—. 2011, ApJ, 736, 19

Brandl, B., Hayward, T. L., Houck, J. R., Gull, G. E., Pirger, B., & Schoenwald, J. 1997, in Society of Photo-Optical Instrumentation Engineers (SPIE) Conference Series, Vol. 3126, Adaptive Optics and Applications, ed. R. K. Tyson & R. Q. Fugate, 515

Burke, C. J., et al. 2014, ApJS, 210, 19

Burruss, R. S., et al. 2014, in Presented at the Society of Photo-Optical Instrumentation Engineers (SPIE) Conference, Vol. 9148, Society of Photo-Optical Instrumentation Engineers (SPIE) Conference Series

Carter, J. A., et al. 2012, Science, 337, 556

Cassan, A., et al. 2012, Nature, 481, 167

Christiansen, J. L., et al. 2013, ApJS, 207, 35

Cumming, A., Butler, R. P., Marcy, G. W., Vogt, S. S., Wright, J. T., & Fischer, D. A. 2008, PASP, 120, 531

Dawson, R. I., & Murray-Clay, R. A. 2013, ApJ, 767, L24

Demarque, P., Woo, J.-H., Kim, Y.-C., & Yi, S. K. 2004, ApJS, 155, 667

Dong, S., Katz, B., & Socrates, A. 2014, ApJ, 781, L5

Dong, S., & Zhu, Z. 2013, ApJ, 778, 53

Dotter, A., Chaboyer, B., Jevremović, D., Kostov, V., Baron, E., & Ferguson, J. W. 2008, ApJS, 178, 89

Dressing, C. D., Adams, E. R., Dupree, A. K., Kulesa, C., & McCarthy, D. 2014, AJ, 148, 78

Fischer, D. A., Marcy, G. W., Butler, R. P., Vogt, S. S., Frink, S., & Apps, K. 2001, ApJ, 551, 1107

Fischer, D. A., et al. 2012, MNRAS, 419, 2900

Fressin, F., et al. 2013, ApJ, 766, 81

Fruchter, A. S., & Hook, R. N. 2002, PASP, 114, 144

Gaudi, B. S. 2010, ArXiv e-prints

Gazak, J. Z., Johnson, J. A., Tonry, J., Dragomir, D., Eastman, J., Mann, A. W., & Agol, E. 2012, Advances in Astronomy, 2012, 30

Gonzalez, G., & Vanture, A. D. 1998, A&A, 339, L29

Hayward, T. L., Brandl, B., Pirger, B., Blacken, C., Gull, G. E., Schoenwald, J., & Houck, J. R. 2001, PASP, 113, 105

Holman, M. J., & Wiegert, P. A. 1999, AJ, 117, 621

Horch, E. P., Howell, S. B., Everett, M. E., & Ciardi, D. R. 2014, ApJ, 795, 60

Howell, S. B., et al. 2014, PASP, 126, 398

Huang, X., Bakos, G. Á., & Hartman, J. D. 2013, MNRAS, 429, 2001

Huber, D., et al. 2014, ApJS, 211, 2

Jenkins, J. M., et al. 2010, ApJ, 713, L87

Kipping, D. M., Huang, X., Nesvorný, D., Torres, G., Buchhave, L. A., Bakos, G. Á., & Schmitt, A. R. 2015, ApJ, 799, L14

Knutson, H. A., et al. 2013, ArXiv e-prints

—. 2014, ApJ, 785, 126

Kurucz, R. L. 1993, SYNTHE spectrum synthesis programs and line data

Lovis, C., et al. 2011, A&A, 528, A112

Mandel, K., & Agol, E. 2002, ApJ, 580, L171

Ngo, H., et al. 2015, ApJ, 800, 138

Oppenheimer, B. R., & Hinkley, S. 2009, ARA&A, 47, 253

Perryman, M. A. C., et al. 2001, A&A, 369, 339

Petigura, E. A., Howard, A. W., & Marcy, G. W. 2013, Proceedings of the National Academy of Sciences

Rasio, F. A., & Ford, E. B. 1996, Science, 274, 954

Ricker, G. R., et al. 2015, Journal of Astronomical Telescopes, Instruments, and Systems, 1, 014003

Rowe, J. F., et al. 2015, ApJS, 217, 16

Santos, N. C., Israelian, G., & Mayor, M. 2004, A&A, 415, 1153

Schmitt, J. R., et al. 2014, AJ, 148, 28

Schwamb, M. E., et al. 2012, ApJ, 754, 129

Sneden, C. A. 1973, PhD thesis, THE UNIVERSITY OF TEXAS AT AUSTIN.

Sousa, S. G., et al. 2008, A&A, 487, 373

Torres, G., et al. 2011, ApJ, 727, 24

Wang, J., Xie, J.-W., Barclay, T., & Fischer, D. A. 2014, ApJ, 783, 4

Wang, J., et al. 2013, ApJ, 776, 10

Winn, J. N. 2010, Exoplanet Transits and Occultations, ed. S. Seager, 55–77

Winn, J. N., Fabrycky, D., Albrecht, S., & Johnson, J. A. 2010, ApJ, 718, L145

Wizinowich, P. L., Acton, D. S., Lai, O., Gathright, J., Lupton, W., & Stomski, P. J. 2000, in Society of Photo-Optical Instrumentation Engineers (SPIE) Conference Series, Vol. 4007, Society of Photo-Optical Instrumentation Engineers (SPIE) Conference Series, ed. P. L. Wizinowich, 2–13

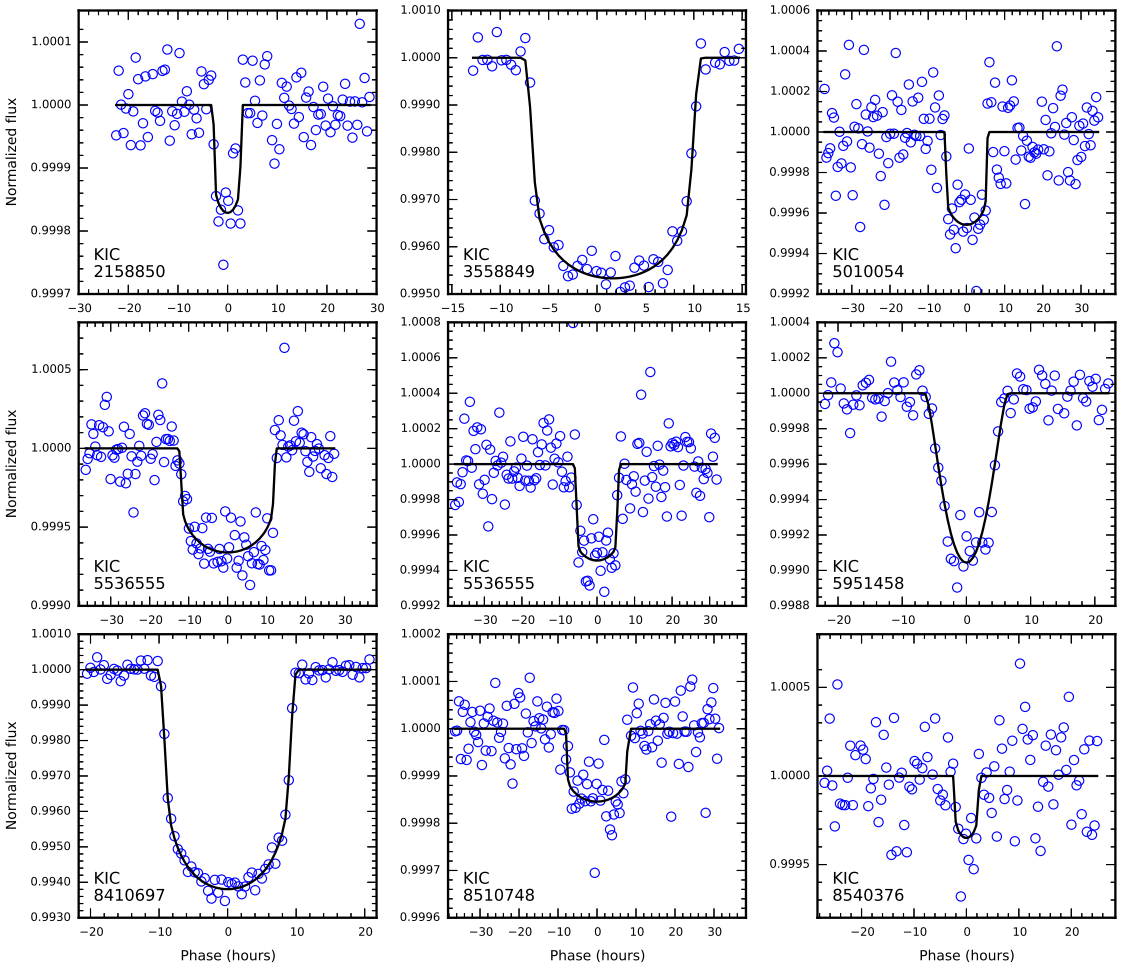

Fig. 1.— Transiting light curves for 1-transit planet candidates. Blue open circles are data points and black solid line is the best-fitting model. Orbital parameters can be found in Table 1.

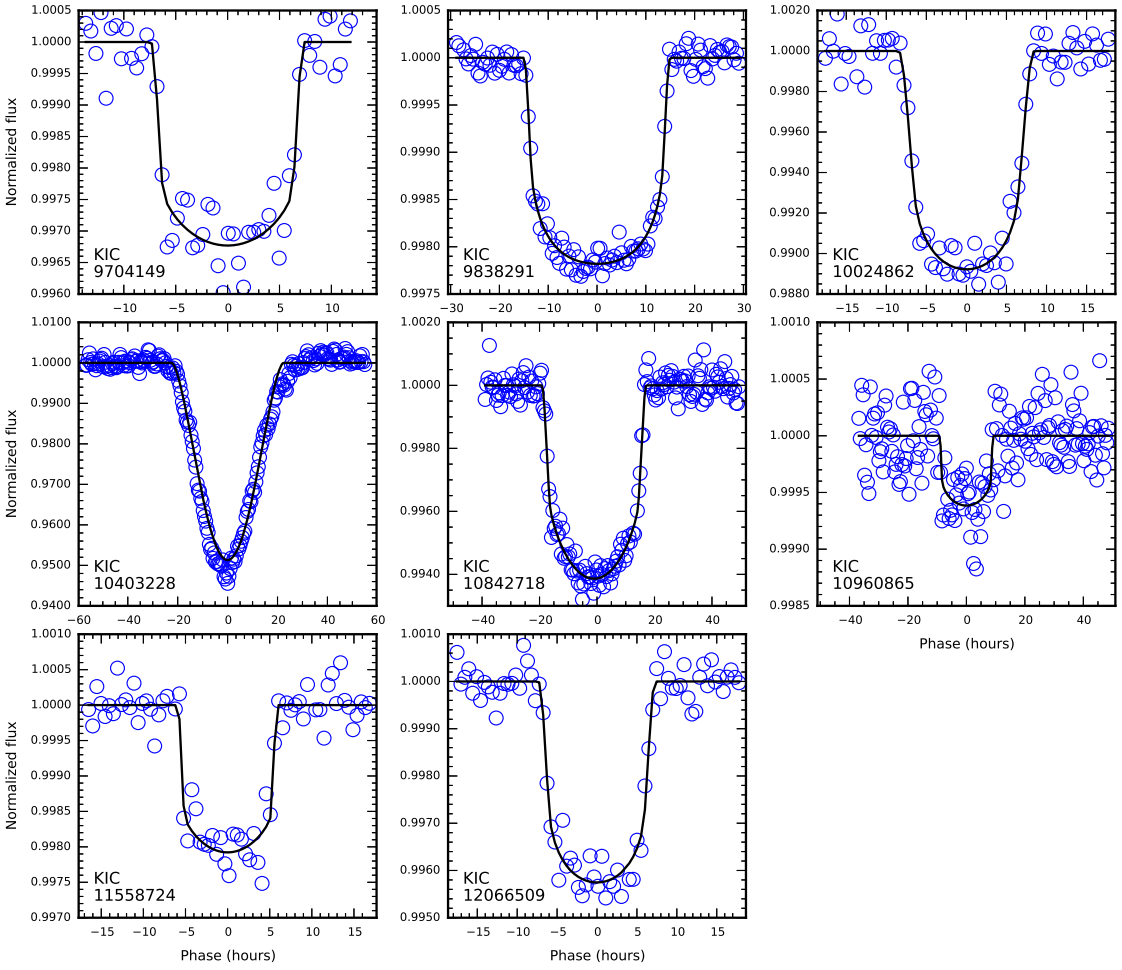

Fig. 2.— Transiting light curves for 1-transit planet candidates. Blue open circles are data points and black solid line is the best-fitting model. Orbital parameters can be found in Table 1.

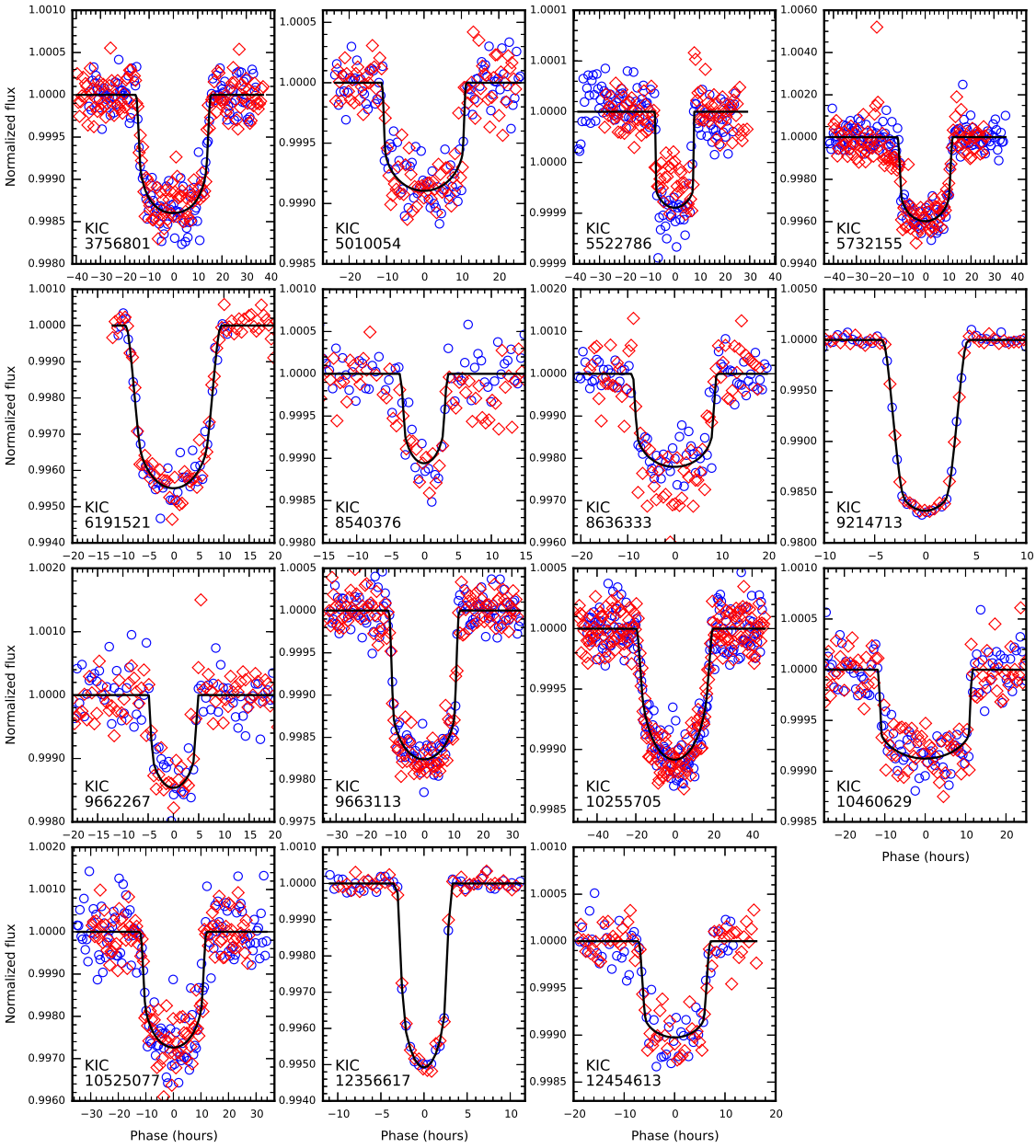

Fig. 3.— Transiting light curves for 2-transit planet candidates. Blue and red open circles are data points for odd- and even-numbered transits. Black solid line is the best-fitting model. Orbital parameters can be found in Table 2.

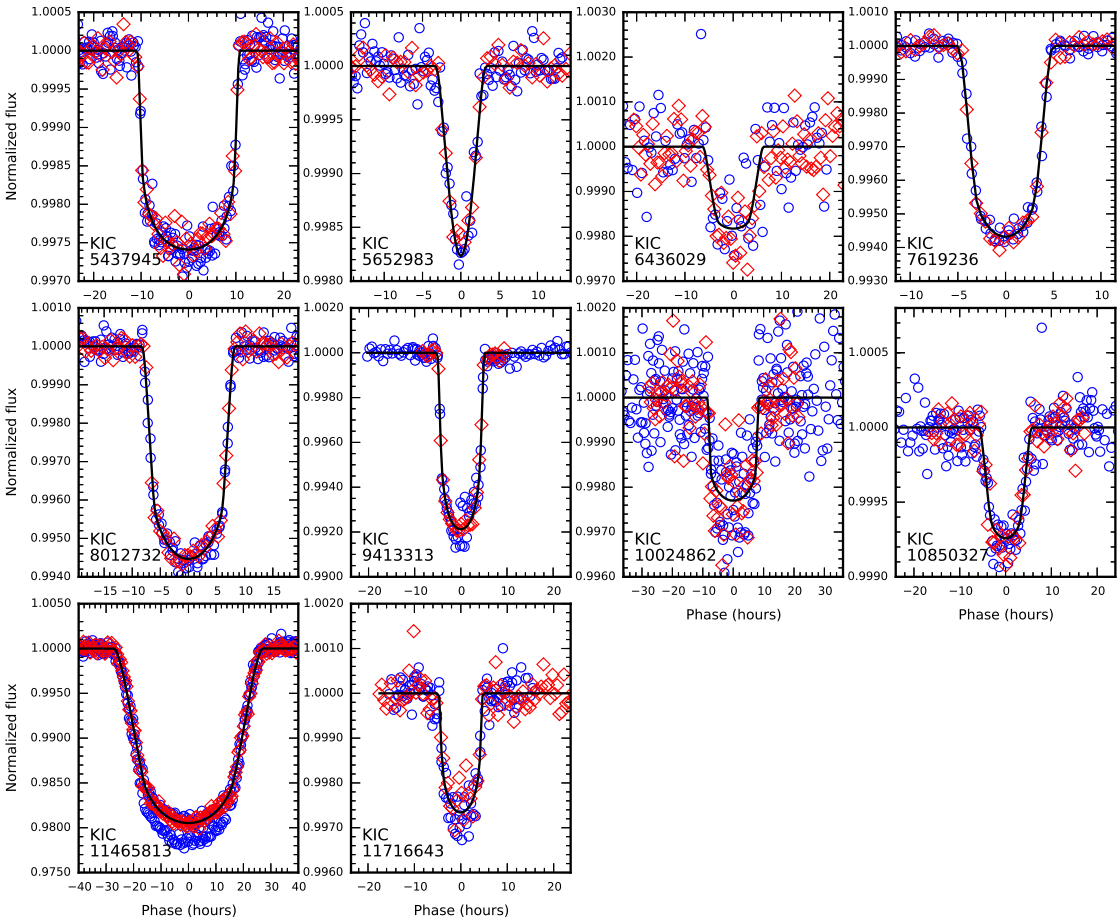

Fig. 4.— Transiting light curves for 3-transit planet candidates. Blue and red open circles are data points for odd- and even-numbered transits. Black solid line is the best-fitting model. Orbital parameters can be found in Table 3.

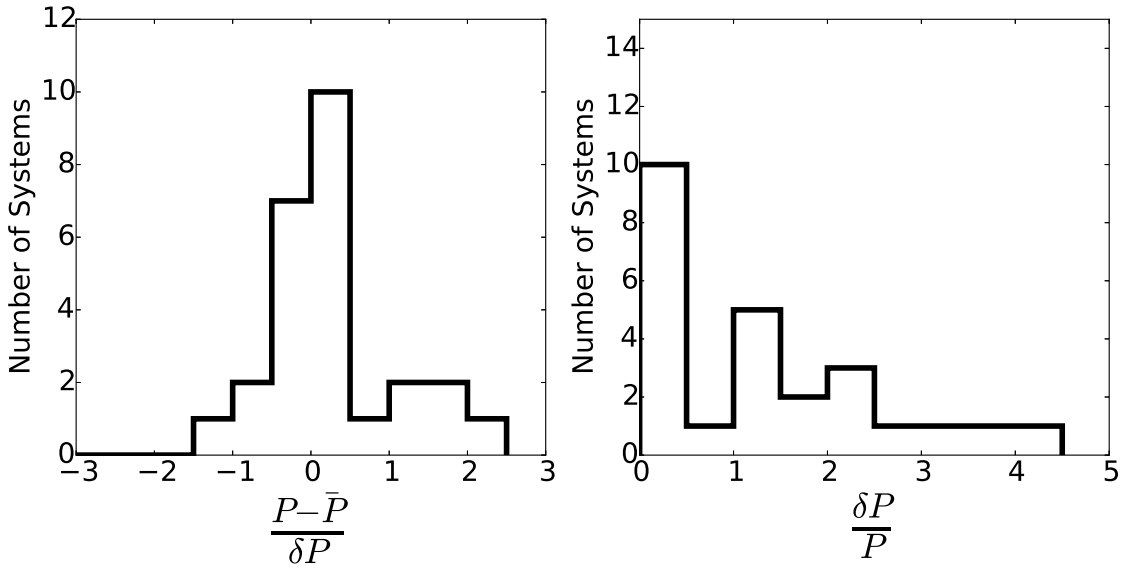

Fig. 5.— Left: distribution of the difference between the period estimated from individual transit ($\bar{P}$) and the period estimated from the time interval of consecutive transits (P) for 25 candidate planetary systems with 2-3 visible transits. The difference is normalized by measurement uncertainty of δP. Right: distribution of the fractional error $\delta P/P$.

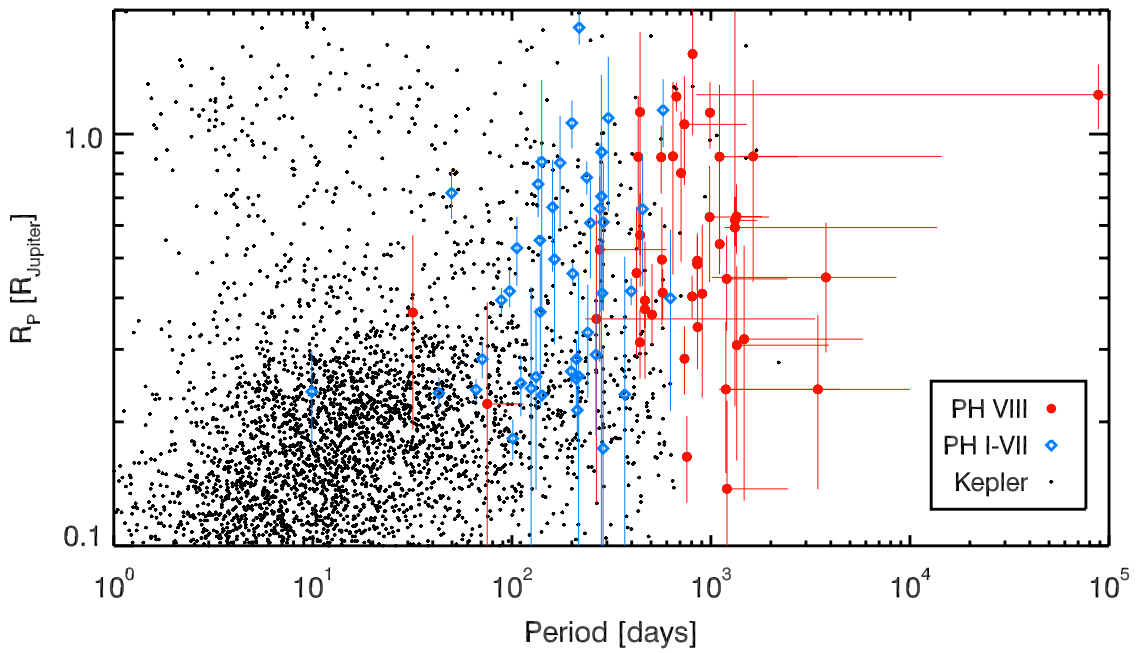

Fig. 6.— Scatter plot of planet radii vs. orbital periods. Black dots are *Kepler* planet candidates. Red filled circles are planet candidates from this work that are identified by Planet Hunters. Blue diamonds are planet candidates from previous Planet Hunters papers. Long-period planet candidates are predominantly discovered by Planet Hunters.

Table 1. Orbital Parameters (1 visible transit)

KIC	KOI	P Mode (days)	P Range (days)	a/R_*	Inclination (deg)	R_P/R_*	R_P ($R_\oplus$)	Epoch (BKJD)	μ_1	μ_2
2158850		1203.8	[1179.3..2441.6]	$1037.9^{+225.7}_{-274.6}$	$89.956^{+0.058}_{-0.110}$	$0.013^{+0.002}_{-0.001}$	$1.6^{+1.0}_{-0.8}$	$411.791^{+0.008}_{-0.008}$	$0.520^{+0.330}_{-0.350}$	$-0.070^{+0.450}_{-0.430}$
3558849	04307	1322.3	[1311.1..1708.4]	$576.7^{+21.5}_{-50.2}$	$89.973^{+0.023}_{-0.031}$	$0.063^{+0.002}_{-0.002}$	$6.9^{+1.0}_{-0.9}$	$279.920^{+0.440}_{-0.300}$	$0.350^{+0.300}_{-0.230}$	$0.220^{+0.370}_{-0.460}$
5010054		1348.2	[1311.2..3913.9]	$825.1^{+134.8}_{-264.2}$	$89.963^{+0.140}_{-0.250}$	$0.021^{+0.002}_{-0.002}$	$3.4^{+1.8}_{-1.6}$	$1500.902^{+0.008}_{-0.009}$	$0.400^{+0.380}_{-0.280}$	$-0.040^{+0.420}_{-0.440}$
5536555		3444.7	[1220.7..9987.4]	$908.4^{+119.4}_{-191.1}$	$89.965^{+0.024}_{-0.038}$	$0.024^{+0.003}_{-0.003}$	$2.7^{+1.4}_{-1.1}$	$370.260^{+0.033}_{-0.038}$	$0.500^{+0.350}_{-0.330}$	$0.070^{+0.430}_{-0.420}$
5536555		1188.4	[1098.6..4450.9]	$431.8^{+71.1}_{-97.8}$	$89.887^{+0.068}_{-0.130}$	$0.024^{+0.002}_{-0.001}$	$2.7^{+1.2}_{-1.0}$	$492.410^{+0.009}_{-0.008}$	$0.510^{+0.340}_{-0.340}$	$-0.140^{+0.410}_{-0.410}$
5951458		1320.1	[1167.6..13721.9]	$278.1^{+109.1}_{-66.0}$	$89.799^{+0.090}_{-0.120}$	$0.040^{+0.089}_{-0.008}$	$6.6^{+26.3}_{-4.2}$	$423.463^{+0.010}_{-0.013}$	$0.520^{+0.330}_{-0.350}$	$0.000^{+0.430}_{-0.420}$
8410697		1104.3	[1048.9..2717.8]	$446.0^{+7.7}_{-17.1}$	$89.976^{+0.024}_{-0.031}$	$0.072^{+0.001}_{-0.001}$	$9.8^{+4.9}_{-4.7}$	$542.122^{+0.001}_{-0.001}$	$0.410^{+0.130}_{-0.130}$	$0.210^{+0.240}_{-0.230}$
8510748		1468.3	[1416.0..5788.4]	$569.5^{+145.4}_{-203.5}$	$89.938^{+0.044}_{-0.073}$	$0.012^{+0.001}_{-0.001}$	$3.6^{+2.4}_{-2.1}$	$1536.548^{+0.013}_{-0.015}$	$0.500^{+0.300}_{-0.300}$	$0.000^{+0.450}_{-0.450}$
8540376		75.2	[74.1..114.1]	$103.9^{+14.1}_{-14.1}$	$89.701^{+0.160}_{-0.160}$	$0.018^{+0.004}_{-0.005}$	$2.4^{+1.9}_{-1.4}$	$1516.911^{+0.020}_{-0.020}$	$0.510^{+0.340}_{-0.340}$	$0.000^{+0.440}_{-0.420}$
9704149		1199.3	[1171.3..2423.2]	$600.9^{+71.2}_{-121.8}$	$89.955^{+0.059}_{-0.076}$	$0.054^{+0.003}_{-0.003}$	$5.0^{+1.4}_{-1.3}$	$419.722^{+0.007}_{-0.007}$	$0.490^{+0.330}_{-0.320}$	$-0.080^{+0.450}_{-0.440}$
9838291		3783.8	[1008.5..8546.1]	$930.4^{+72.1}_{-97.5}$	$89.974^{+0.069}_{-0.063}$	$0.043^{+0.001}_{-0.001}$	$5.1^{+1.8}_{-1.8}$	$582.559^{+0.003}_{-0.004}$	$0.280^{+0.250}_{-0.180}$	$0.430^{+0.280}_{-0.370}$
10024862		735.7	[713.0..1512.8]	$324.1^{+41.2}_{-36.2}$	$89.905^{+0.030}_{-0.022}$	$0.098^{+0.004}_{-0.004}$	$11.8^{+3.7}_{-3.4}$	$878.561^{+0.004}_{-0.004}$	$0.370^{+0.310}_{-0.250}$	$0.280^{+0.370}_{-0.500}$
10403228		88418.1	[846.5..103733.3]	$13877.4^{+400.0}_{-408.4}$	$89.996^{+0.011}_{-0.009}$	$0.269^{+0.022}_{-0.024}$	$9.7^{+2.4}_{-2.2}$	$744.843^{+0.013}_{-0.013}$	$0.550^{+0.310}_{-0.370}$	$0.050^{+0.420}_{-0.410}$
10842718		1629.2	[1364.7..14432.2]	$347.5^{+19.8}_{-23.9}$	$89.938^{+0.010}_{-0.008}$	$0.071^{+0.002}_{-0.002}$	$9.9^{+5.4}_{-5.0}$	$226.300^{+1.100}_{-0.520}$	$0.700^{+0.180}_{-0.240}$	$-0.150^{+0.400}_{-0.300}$
10960865		265.8	[233.7..3335.9]	$99.7^{+13.7}_{-28.6}$	$89.703^{+0.240}_{-0.530}$	$0.024^{+0.003}_{-0.003}$	$3.9^{+3.0}_{-2.5}$	$1507.959^{+0.007}_{-0.006}$	$0.510^{+0.330}_{-0.340}$	$-0.010^{+0.450}_{-0.450}$
11558724		276.1	[267.0..599.3]	$181.1^{+10.1}_{-25.8}$	$89.897^{+0.021}_{-0.032}$	$0.043^{+0.002}_{-0.002}$	$5.9^{+2.9}_{-2.7}$	$915.196^{+0.003}_{-0.003}$	$0.470^{+0.330}_{-0.310}$	$-0.130^{+0.460}_{-0.430}$
12066509		984.6	[959.0..1961.7]	$460.8^{+89.4}_{-72.3}$	$89.925^{+0.050}_{-0.036}$	$0.062^{+0.003}_{-0.003}$	$7.1^{+2.3}_{-2.2}$	$632.090^{+0.004}_{-0.004}$	$0.360^{+0.330}_{-0.250}$	$0.240^{+0.390}_{-0.500}$

Table 2. Orbital Parameters (2 visible transits)

KIC	KOI	P (days)	a/R_*	Inclination (deg)	R_P/R_*	R_P ($R_\oplus$)	Epoch (BKJD)	μ_1	μ_2
3756801	01206	$422.91360^{+0.01608}_{-0.01603}$	$92.2^{+21.0}_{-27.0}$	$89.620^{+0.280}_{-0.360}$	$0.036^{+0.003}_{-0.002}$	$5.1^{+2.2}_{-1.9}$	$448.494^{+0.008}_{-0.008}$	$0.260^{+0.310}_{-0.180}$	$0.410^{+0.340}_{-0.500}$
5010054†		$904.20180^{+0.01339}_{-0.01212}$	$291.9^{+26.0}_{-62.0}$	$89.918^{+0.057}_{-0.093}$	$0.028^{+0.001}_{-0.001}$	$4.6^{+2.2}_{-2.0}$	$356.412^{+0.009}_{-0.008}$	$0.460^{+0.330}_{-0.310}$	$0.050^{+0.440}_{-0.450}$
5522786†		$757.09520^{+0.01176}_{-0.01211}$	$330.3^{+45.0}_{-77.0}$	$89.913^{+0.062}_{-0.083}$	$0.009^{+0.001}_{-0.001}$	$1.9^{+0.4}_{-0.3}$	$282.995^{+0.009}_{-0.008}$	$0.320^{+0.360}_{-0.230}$	$-0.060^{+0.360}_{-0.400}$
5732155†		$644.21470^{+0.01424}_{-0.01598}$	$204.3^{+15.0}_{-31.0}$	$89.894^{+0.073}_{-0.100}$	$0.059^{+0.002}_{-0.002}$	$9.9^{+5.2}_{-4.7}$	$536.702^{+0.006}_{-0.005}$	$0.410^{+0.320}_{-0.270}$	$0.040^{+0.440}_{-0.460}$
6191521	00847	$1106.24040^{+0.00922}_{-0.00954}$	$326.6^{+30.0}_{-26.0}$	$89.862^{+0.020}_{-0.020}$	$0.068^{+0.002}_{-0.002}$	$6.0^{+0.8}_{-0.6}$	$382.949^{+0.007}_{-0.008}$	$0.480^{+0.340}_{-0.320}$	$0.150^{+0.390}_{-0.400}$
8540376		$31.80990^{+0.00919}_{-0.00933}$	$34.7^{+3.7}_{-6.9}$	$89.300^{+0.490}_{-0.720}$	$0.030^{+0.002}_{-0.002}$	$4.1^{+2.2}_{-1.9}$	$1520.292^{+0.006}_{-0.006}$	$0.570^{+0.300}_{-0.350}$	$0.030^{+0.440}_{-0.420}$
8636333	03349	$804.71420^{+0.01301}_{-0.01500}$	$343.8^{+21.0}_{-52.0}$	$89.946^{+0.038}_{-0.062}$	$0.044^{+0.002}_{-0.002}$	$4.5^{+0.5}_{-0.5}$	$271.889^{+0.009}_{-0.012}$	$0.420^{+0.340}_{-0.280}$	$0.080^{+0.430}_{-0.470}$
9214713†	00422	$809.01370^{+0.00156}_{-0.00152}$	$637.2^{+16.0}_{-14.0}$	$89.933^{+0.004}_{-0.003}$	$0.131^{+0.002}_{-0.002}$	$17.5^{+6.6}_{-6.4}$	$250.635^{+0.001}_{-0.001}$	$0.480^{+0.350}_{-0.340}$	$-0.160^{+0.430}_{-0.430}$
9662267†		$466.19580^{+0.00850}_{-0.00863}$	$357.1^{+37.0}_{-82.0}$	$89.931^{+0.049}_{-0.081}$	$0.035^{+0.002}_{-0.002}$	$4.5^{+1.7}_{-1.6}$	$481.883^{+0.006}_{-0.006}$	$0.590^{+0.280}_{-0.350}$	$-0.060^{+0.460}_{-0.440}$
9663113	00179	$572.38470^{+0.00583}_{-0.00567}$	$153.5^{+23.0}_{-15.0}$	$89.768^{+0.095}_{-0.062}$	$0.041^{+0.001}_{-0.001}$	$4.6^{+0.6}_{-0.7}$	$306.506^{+0.004}_{-0.004}$	$0.450^{+0.330}_{-0.270}$	$0.040^{+0.390}_{-0.420}$
10255705†		$707.78500^{+0.01844}_{-0.01769}$	$92.1^{+27.0}_{-11.0}$	$89.510^{+0.210}_{-0.110}$	$0.034^{+0.002}_{-0.003}$	$8.9^{+3.6}_{-3.5}$	$545.741^{+0.014}_{-0.013}$	$0.620^{+0.250}_{-0.350}$	$0.250^{+0.350}_{-0.280}$
10460629	01168	$856.67100^{+0.01133}_{-0.01039}$	$275.4^{+15.0}_{-40.0}$	$89.932^{+0.048}_{-0.075}$	$0.028^{+0.001}_{-0.001}$	$3.8^{+0.8}_{-0.8}$	$228.451^{+0.008}_{-0.006}$	$0.420^{+0.320}_{-0.280}$	$-0.070^{+0.420}_{-0.420}$
10525077	05800	$854.08300^{+0.01628}_{-0.01697}$	$239.3^{+46.0}_{-52.0}$	$89.861^{+0.096}_{-0.098}$	$0.050^{+0.003}_{-0.003}$	$5.5^{+0.9}_{-0.8}$	$335.236^{+0.012}_{-0.012}$	$0.500^{+0.310}_{-0.310}$	$0.140^{+0.410}_{-0.430}$
10525077	05800	$427.04150^{+0.01487}_{-0.01628}$	$130.9^{+14.0}_{-30.0}$	$89.800^{+0.140}_{-0.220}$	$0.049^{+0.003}_{-0.002}$	$5.4^{+0.9}_{-0.8}$	$335.238^{+0.011}_{-0.012}$	$0.500^{+0.310}_{-0.310}$	$0.160^{+0.410}_{-0.440}$
12356617	00375	$988.88111^{+0.00137}_{-0.00146}$	$1059.5^{+29.0}_{-53.0}$	$89.966^{+0.003}_{-0.004}$	$0.069^{+0.001}_{-0.001}$	$12.5^{+2.4}_{-2.3}$	$239.224^{+0.001}_{-0.001}$	$0.650^{+0.230}_{-0.320}$	$-0.050^{+0.460}_{-0.330}$
12454613†		$736.37700^{+0.01531}_{-0.01346}$	$257.0^{+140.0}_{-50.0}$	$89.820^{+0.120}_{-0.064}$	$0.033^{+0.002}_{-0.002}$	$3.2^{+0.6}_{-0.6}$	$490.271^{+0.014}_{-0.012}$	$0.460^{+0.360}_{-0.310}$	$-0.030^{+0.450}_{-0.430}$

Note. — All targets have AO imaging observations. The detections and detection limits are given in Table 6 and Table 5. Targets with follow-up spectroscopic observations are marked with an †.

Table 3. Orbital Parameters (3 visible transits)

KIC	**KOI**	**P (days)**	a/R_*	**Inclination (deg)**	R_P/R_*	R_P ($R_\oplus$)	**Epoch (BKJD)**	μ_1	μ_2
5437945	03791	$440.78130^{+0.00563}_{-0.00577}$	$158.9^{+5.1}_{-12.0}$	$89.904^{+0.066}_{-0.086}$	$0.047^{+0.001}_{-0.001}$	$6.4^{+1.6}_{-1.6}$	$139.355^{+0.003}_{-0.003}$	$0.320^{+0.180}_{-0.160}$	$0.290^{+0.270}_{-0.290}$
5652983	00371	$498.38960^{+0.01166}_{-0.01131}$	$215.8^{+29.0}_{-33.0}$	$89.721^{+0.049}_{-0.072}$	$0.111^{+0.061}_{-0.057}$	$35.9^{+24.7}_{-20.0}$	$244.083^{+0.008}_{-0.008}$	$0.550^{+0.310}_{-0.360}$	$0.000^{+0.420}_{-0.430}$
6436029	02828	$505.45900^{+0.04500}_{-0.04102}$	$155.5^{+32.0}_{-39.0}$	$89.661^{+0.072}_{-0.150}$	$0.047^{+0.012}_{-0.005}$	$4.1^{+1.3}_{-0.7}$	$458.092^{+0.035}_{-0.031}$	$0.510^{+0.340}_{-0.360}$	$0.000^{+0.430}_{-0.440}$
7619236†	00682	$562.70945^{+0.00411}_{-0.00399}$	$311.9^{+16.0}_{-14.0}$	$89.851^{+0.012}_{-0.011}$	$0.077^{+0.002}_{-0.002}$	$9.9^{+1.9}_{-1.8}$	$185.997^{+0.002}_{-0.002}$	$0.410^{+0.370}_{-0.280}$	$0.230^{+0.360}_{-0.440}$
8012732†		$431.46810^{+0.00358}_{-0.00365}$	$160.2^{+5.4}_{-4.6}$	$89.741^{+0.018}_{-0.015}$	$0.074^{+0.001}_{-0.002}$	$9.8^{+4.1}_{-3.9}$	$391.807^{+0.002}_{-0.002}$	$0.560^{+0.290}_{-0.320}$	$0.000^{+0.430}_{-0.360}$
9413313†		$440.39840^{+0.00275}_{-0.00282}$	$352.1^{+7.2}_{-15.0}$	$89.966^{+0.023}_{-0.028}$	$0.080^{+0.001}_{-0.001}$	$12.6^{+7.2}_{-6.9}$	$485.608^{+0.002}_{-0.002}$	$0.380^{+0.130}_{-0.130}$	$0.450^{+0.200}_{-0.250}$
10024862†		$567.04450^{+0.02557}_{-0.02936}$	$230.9^{+37.0}_{-81.0}$	$89.868^{+0.095}_{-0.190}$	$0.046^{+0.003}_{-0.003}$	$5.5^{+2.0}_{-1.6}$	$359.666^{+0.017}_{-0.021}$	$0.410^{+0.370}_{-0.280}$	$0.070^{+0.430}_{-0.480}$
10850327	05833	$440.16700^{+0.01738}_{-0.01671}$	$124.9^{+36.0}_{-21.0}$	$89.570^{+0.120}_{-0.100}$	$0.032^{+0.003}_{-0.003}$	$3.5^{+0.7}_{-0.6}$	$470.358^{+0.011}_{-0.011}$	$0.570^{+0.310}_{-0.370}$	$0.120^{+0.390}_{-0.360}$
11465813	00771	$670.65020^{+0.01018}_{-0.01018}$	$85.2^{+1.1}_{-1.1}$	$89.535^{+0.013}_{-0.012}$	$0.136^{+0.002}_{-0.002}$	$13.8^{+1.1}_{-1.1}$	$209.041^{+0.004}_{-0.004}$	$0.420^{+0.260}_{-0.240}$	$0.340^{+0.360}_{-0.380}$
11716643†	05929	$466.00010^{+0.00799}_{-0.00775}$	$380.5^{+24.0}_{-61.0}$	$89.947^{+0.037}_{-0.059}$	$0.047^{+0.002}_{-0.002}$	$4.2^{+0.5}_{-0.4}$	$434.999^{+0.005}_{-0.005}$	$0.490^{+0.280}_{-0.290}$	$0.230^{+0.370}_{-0.420}$

Note. — All targets have AO imaging observations. The detections and detection limits are given in Table 6 and Table 5. Targets marked with a † are systems displaying TTVs.

Table 4. Stellar Parameters

KIC	KOI	α (h m s)	δ (d m s)	Kp (mag)	$T_{\rm eff}$ (K)	$\log g$ (cgs)	[Fe/H] (dex)	M_* ($M_\odot$)	R_* ($R_\odot$)
2158850		19 24 37.875	+37 30 55.69	10.9	6108^{+203}_{-166}	$4.48^{+0.14}_{-0.60}$	$-1.96^{+0.34}_{-0.26}$	[0.72..0.96]	[0.63..1.54]
3558849	04307	19 39 47.962	+38 36 18.68	14.2	6175^{+168}_{-194}	$4.44^{+0.07}_{-0.27}$	$-0.42^{+0.28}_{-0.30}$	[0.87..1.09]	[0.90..1.11]
3644071	01192	19 24 07.718	+38 42 14.08	14.2	5609^{+159}_{-141}	$4.35^{+0.15}_{-0.23}$	$-0.04^{+0.26}_{-0.24}$	[0.85..1.04]	[0.81..1.05]
3756801	01206	19 35 49.102	+38 53 59.89	13.6	5796^{+162}_{-165}	$4.12^{+0.26}_{-0.22}$	$-0.02^{+0.24}_{-0.28}$	[0.89..1.19]	[0.87..1.75]
5010054†		19 25 59.610	+40 10 58.40	14.0	6300^{+400}_{-400}	$4.30^{+0.50}_{-0.50}$	$0.02^{+0.22}_{-0.28}$	[0.87..1.32]	[0.87..2.13]
5437945	03791	19 13 53.962	+40 39 04.90	13.8	6340^{+176}_{-199}	$4.16^{+0.22}_{-0.25}$	$-0.38^{+0.28}_{-0.30}$	[0.90..1.24]	[0.95..1.53]
5522786†		19 13 22.440	+40 43 52.75	9.3	8600^{+300}_{-300}	$4.20^{+0.20}_{-0.20}$	$0.07^{+0.14}_{-0.59}$	[1.86..2.19]	[1.63..2.12]
5536555		19 30 57.482	+40 44 10.97	13.5	5996^{+155}_{-159}	$4.49^{+0.06}_{-0.28}$	$-0.48^{+0.30}_{-0.26}$	[0.69..0.98]	[0.67..1.38]
5652983	00371	19 58 42.276	+40 51 23.36	12.2	5198^{+95}_{-95}	$3.61^{+0.02}_{-0.02}$	...	[1.13..1.61]	[2.70..3.23]
5732155†		19 53 42.132	+40 54 23.76	15.2	6000^{+400}_{-400}	$4.20^{+0.50}_{-0.50}$	$-0.04^{+0.22}_{-0.30}$	[0.87..1.33]	[0.82..2.25]
5951458		19 15 57.979	+41 13 22.91	12.7	6258^{+170}_{-183}	$4.08^{+0.28}_{-0.23}$	$-0.50^{+0.30}_{-0.30}$	[0.77..1.19]	[0.70..2.34]
6191521	00847	19 08 37.032	+41 33 56.84	15.2	5665^{+181}_{-148}	$4.56^{+0.05}_{-0.27}$	$-0.58^{+0.34}_{-0.26}$	[0.77..0.92]	[0.75..0.88]
6436029	02828	19 18 09.317	+41 53 34.15	15.8	4817^{+181}_{-131}	$4.50^{+0.08}_{-0.84}$	$0.42^{+0.06}_{-0.24}$	[0.79..0.88]	[0.75..0.84]
7619236	00682	19 40 47.518	+43 16 10.24	13.9	5589^{+102}_{-108}	$4.23^{+0.13}_{-0.12}$	$0.34^{+0.10}_{-0.14}$	[0.93..1.12]	[0.98..1.36]
8012732		18 58 55.079	+43 51 51.18	13.9	6221^{+166}_{-249}	$4.29^{+0.12}_{-0.38}$	$0.20^{+0.16}_{-0.32}$	[0.77..1.07]	[0.75..1.69]
8410697		18 48 44.594	+44 26 04.13	13.4	5918^{+157}_{-152}	$4.37^{+0.14}_{-0.24}$	$-0.42^{+0.30}_{-0.26}$	[0.74..1.08]	[0.66..1.85]
8510748		19 48 19.891	+44 30 56.12	11.6	7875^{+233}_{-309}	$3.70^{+0.28}_{-0.10}$	$0.04^{+0.17}_{-0.38}$	[1.36..2.40]	[1.20..4.23]
8540376		18 49 30.607	+44 41 40.52	14.3	6474^{+178}_{-267}	$4.31^{+0.10}_{-0.33}$	$-0.16^{+0.23}_{-0.32}$	[0.84..1.23]	[0.70..1.82]
8636333	03349	19 43 47.585	+44 45 11.23	15.3	6247^{+175}_{-202}	$4.49^{+0.04}_{-0.27}$	$-0.34^{+0.26}_{-0.30}$	[0.86..1.03]	[0.87..1.01]
9214713†	00422	19 21 33.559	+45 39 55.19	14.7	6200^{+400}_{-400}	$4.40^{+0.50}_{-0.50}$	$-0.30^{+0.26}_{-0.30}$	[0.84..1.17]	[0.79..1.66]
9413313		19 41 40.915	+45 54 12.56	14.1	5359^{+167}_{-143}	$4.40^{+0.13}_{-0.39}$	$0.02^{+0.28}_{-0.26}$	[0.72..1.17]	[0.66..2.24]
9662267†		19 47 10.274	+46 20 59.68	14.9	6000^{+400}_{-400}	$4.50^{+0.50}_{-0.50}$	$-0.06^{+0.22}_{-0.30}$	[0.88..1.21]	[0.79..1.52]
9663113	00179	19 48 10.901	+46 19 43.32	14.0	6065^{+155}_{-180}	$4.42^{+0.08}_{-0.26}$	$-0.28^{+0.28}_{-0.30}$	[0.85..1.10]	[0.91..1.15]
9704149		19 16 39.269	+46 25 18.48	15.1	5897^{+155}_{-169}	$4.53^{+0.03}_{-0.28}$	$-0.16^{+0.24}_{-0.30}$	[0.73..0.99]	[0.67..1.02]
9838291		19 39 02.134	+46 40 39.11	12.9	6123^{+141}_{-177}	$4.47^{+0.05}_{-0.29}$	$-0.14^{+0.22}_{-0.30}$	[0.76..1.08]	[0.72..1.42]
10024862		19 47 12.602	+46 56 04.42	15.9	6616^{+169}_{-358}	$4.33^{+0.08}_{-0.31}$	$0.07^{+0.19}_{-0.39}$	[0.89..1.24]	[0.82..1.39]
10207400		19 26 42.490	+47 15 18.18	15.0	5896^{+154}_{-175}	$4.52^{+0.03}_{-0.23}$	$-0.08^{+0.20}_{-0.30}$	[0.74..0.96]	[0.70..0.98]
10255705†		18 51 24.912	+47 22 38.89	12.9	5300^{+300}_{-300}	$3.80^{+0.40}_{-0.40}$	$-0.12^{+0.33}_{-0.30}$	[0.98..1.40]	[1.62..3.23]
10403228††		19 24 54.410	+47 32 59.93	16.1	3386^{+50}_{-50}	$4.92^{+0.06}_{-0.07}$	$0.00^{+0.10}_{-0.10}$	[0.27..0.37]	[0.28..0.38]
10460629	01168	19 10 20.830	+47 36 00.07	14.0	6449^{+163}_{-210}	$4.23^{+0.16}_{-0.27}$	$-0.32^{+0.24}_{-0.30}$	[0.94..1.29]	[1.02..1.47]
10525077	05800	19 09 30.737	+47 46 16.28	15.4	6091^{+164}_{-213}	$4.42^{+0.06}_{-0.30}$	$-0.04^{+0.22}_{-0.30}$	[0.89..1.13]	[0.91..1.11]
10842718		18 47 47.285	+48 13 21.36	14.6	5754^{+159}_{-156}	$4.38^{+0.12}_{-0.24}$	$-0.06^{+0.26}_{-0.26}$	[0.74..1.12]	[0.65..1.90]
10850327	05833	19 06 21.895	+48 13 12.97	13.0	6277^{+155}_{-187}	$4.43^{+0.07}_{-0.28}$	$-0.46^{+0.28}_{-0.30}$	[0.87..1.10]	[0.90..1.10]
10960865		18 52 52.675	+48 26 40.13	14.2	5547^{+196}_{-154}	$4.05^{+0.34}_{-0.26}$	$0.02^{+0.26}_{-0.26}$	[0.73..1.19]	[0.62..2.42]
11465813	00771	19 46 47.666	+49 18 59.33	15.2	5520^{+83}_{-110}	$4.47^{+0.04}_{-0.14}$	$0.48^{+0.08}_{-0.16}$	[0.88..1.03]	[0.87..0.99]
11558724		19 26 34.094	+49 33 14.65	14.7	6462^{+177}_{-270}	$4.32^{+0.10}_{-0.35}$	$-0.08^{+0.22}_{-0.32}$	[0.81..1.22]	[0.70..1.80]
11716643	05929	19 35 27.665	+49 48 01.04	14.7	5830^{+155}_{-164}	$4.54^{+0.03}_{-0.28}$	$-0.14^{+0.24}_{-0.28}$	[0.79..0.93]	[0.77..0.87]
12066509		19 36 12.245	+50 30 56.09	14.7	6108^{+149}_{-192}	$4.47^{+0.04}_{-0.30}$	$0.07^{+0.15}_{-0.33}$	[0.80..1.11]	[0.76..1.32]
12356617	00375	19 24 48.286	+51 08 39.41	13.3	5755^{+112}_{-112}	$4.10^{+0.14}_{-0.13}$	$0.24^{+0.14}_{-0.14}$	[0.98..1.25]	[1.39..1.96]
12454613†		19 12 40.656	+51 22 55.88	13.5	5500^{+280}_{-280}	$4.60^{+0.30}_{-0.30}$	$0.00^{+0.24}_{-0.24}$	[0.82..1.00]	[0.77..1.00]

Note. — Targets with follow-up spectroscopic observations are marked with an †. Their stellar properties are based on MOOG analysis. We report 1-σ range for stellar mass and radius. ††: Stellar mass and radius are adopted from Huber et al. (2014).

Table 5. AO Sensitivity to Companions

		Kepler					Observation			Limiting Delta Magnitude					
KIC	**KOI**	**Kmag** [mag]	i [mag]	J [mag]	H [mag]	K [mag]	**Companion within 5″**	**Instrument**	**Filter**	**0.1** [″]	**0.2** [″]	**0.5** [″]	**1.0** [″]	**2.0** [″]	**4.0** [″]
3756801	01206	13.642	13.408	12.439	12.099	12.051	no	NIRC2	K	2.1	4.2	5.2	5.3	5.3	5.3
5010054		13.961	13.710	12.797	12.494	12.412	no	NIRC2	K	2.0	3.9	4.9	5.0	4.9	4.9
5010054		13.961	13.710	12.797	12.494	12.412	no	Robo-AO	i	0.2	0.5	2.3	3.8	4.6	4.7
5437945	03791	13.771	13.611	12.666	12.429	12.367	no	NIRC2	J	2.4	3.5	5.3	5.7	5.7	5.7
5437945	03791	13.771	13.611	12.666	12.429	12.367	no	NIRC2	K	2.8	4.6	6.3	6.9	7.0	6.9
5522786		9.350	9.572	9.105	9.118	9.118	no	NIRC2	K	1.5	4.6	5.9	6.5	6.5	6.5
5522786		9.350	9.572	9.105	9.118	9.118	no	Robo-AO	i	0.0	0.4	2.7	4.6	6.9	8.0
5652983	00371	12.193	11.895	10.723	10.289	10.169	no	NIRC2	K	2.2	4.2	5.5	5.7	5.8	5.7
5732155		15.195	14.978	14.006	13.705	13.621	yes	NIRC2	K	2.1	3.5	4.8	4.9	5.0	5.0
5732155		15.195	14.978	14.006	13.705	13.621	no	Robo-AO	i	0.6	0.9	2.2	3.2	3.4	3.6
6191521	00847	15.201	14.970	13.935	13.585	13.569	no	NIRC2	K	2.0	3.7	4.9	5.1	5.1	5.1
6436029	02828	15.768	15.369	14.041	13.506	13.429	no	NIRC2	K	1.2	2.7	4.4	4.7	4.7	4.6
7619236	00682	13.916	13.692	12.688	12.378	12.260	no	NIRC2	K	1.8	3.8	4.8	5.0	5.0	4.9
8012732		13.922	13.727	13.094	12.794	12.790	no	Robo-AO	i	0.2	0.5	1.8	3.5	4.3	4.3
8540376		14.294	14.151	13.259	13.013	12.965	no	Robo-AO	i	0.2	0.4	1.9	3.4	4.1	4.2
8636333	03349	15.292	15.113	14.192	13.890	13.880	yes	NIRC2	H	1.0	2.0	3.6	4.8	5.0	5.0
8636333	03349	15.292	15.113	14.192	13.890	13.880	yes	NIRC2	K	1.0	2.3	3.9	4.6	4.7	4.6
9214713	00422	14.740	14.562	13.608	13.385	13.304	no	NIRC2	K	2.4	3.8	5.3	5.5	5.5	5.5
9413313		14.116	13.835	12.733	12.335	12.227	no	NIRC2	K	1.9	3.7	4.8	4.9	4.9	4.9
9413313		14.116	13.835	12.733	12.335	12.227	no	Robo-AO	i	0.4	0.7	2.4	3.5	3.9	3.9
9662267		14.872	14.667	13.670	13.385	13.339	no	NIRC2	K	1.6	3.4	4.9	5.0	5.1	5.1
9662267		14.872	14.667	13.670	13.385	13.339	no	Robo-AO	i	0.4	0.6	2.4	3.2	3.8	3.8
9663113	00179	13.955	13.765	12.823	12.545	12.502	no	NIRC2	K	2.2	3.9	4.8	4.9	4.9	4.9
9704149		15.102	14.897	13.896	13.538	13.454	no	NIRC2	K	1.7	3.2	4.4	4.7	4.8	4.7
9704149		15.102	14.897	13.896	13.538	13.454	no	Robo-AO	i	0.6	0.8	2.1	3.1	3.5	3.5
10024862		15.881	15.712	14.846	14.551	14.541	no	NIRC2	K	0.7	1.8	2.2	2.2	2.2	2.3
10024862		15.881	15.712	14.846	14.551	14.541	no	Robo-AO	i	0.8	1.1	2.0	2.6	2.8	2.8
10255705		12.950	12.678	11.560	11.105	11.021	yes	NIRC2	H	2.5	4.0	5.8	6.1	6.3	6.2
10255705		12.950	12.678	11.560	11.105	11.021	yes	NIRC2	J	2.0	3.3	5.2	5.6	5.7	5.7
10255705		12.950	12.678	11.560	11.105	11.021	yes	NIRC2	K	2.4	4.2	5.6	5.7	5.8	5.8
10255705		12.950	12.678	11.560	11.105	11.021	yes	Robo-AO	i	0.2	0.3	1.7	3.1	4.6	5.0
10460629	01168	13.997	13.851	12.923	12.672	12.595	no	NIRC2	K	2.1	3.7	4.7	4.8	4.7	4.7
10525077	05800	15.355	15.163	14.143	13.868	13.753	no	NIRC2	K	1.9	3.4	4.5	4.8	4.8	4.8
10850327	05833	13.014	12.872	11.993	11.711	11.666	no	NIRC2	K	2.4	4.1	5.1	5.4	5.4	5.3
11465813	00771	15.207	15.068	13.678	13.317	13.253	yes	NIRC2	H	1.0	2.5	4.7	5.2	5.0	5.2
11465813	00771	15.207	15.068	13.678	13.317	13.253	yes	NIRC2	J	0.9	2.0	4.2	4.6	4.6	4.7
11465813	00771	15.207	15.068	13.678	13.317	13.253	yes	NIRC2	K	1.5	3.2	4.1	4.2	4.3	4.3
11716643	05929	14.692	14.485	13.483	13.095	13.092	no	NIRC2	K	2.1	3.4	4.2	4.3	4.3	4.3
12356617	00375	13.293	13.111	12.137	11.842	11.791	yes	PHARO	K	0.1	0.8	2.5	4.0	4.9	5.0
12454613		13.537	13.306	12.326	11.929	11.867	no	NIRC2	K	2.0	4.2	5.3	5.4	5.5	5.5
12454613		13.537	13.306	12.326	11.929	11.867	no	Robo-AO	i	0.3	0.4	1.8	3.4	4.5	4.7

Table 6. AO Detections

		Kepler							Companion			
KIC	**KOI**	**Kmag** [mag]	i [mag]	J [mag]	H [mag]	K [mag]	**sep.** [$''$]	**P.A.** [deg]	Δi [mag]	ΔJ [mag]	ΔH [mag]	ΔK [mag]
5732155		15.195	14.978	14.006	13.705	13.621	0.93	220.8				4.94
8636333	03349	15.292	15.113	14.192	13.890	13.880	0.32	265.9			1.58	1.71
10255705		12.950	12.678	11.560	11.105	11.021	1.07	163.8	1.94	2.27	2.37	2.40
11465813	00771	15.207	15.068	13.678	13.317	13.253	1.78	282.4		0.77	0.74	0.65
12356617	00375	13.293	13.111	12.137	11.842	11.791	3.12	305.1				4.42